J Mater Sci (2007) 42:812–816
DOI 10.1007/s10853-006-0143-3

Dielectric responses in $Mg_{1/3}Ta_{2/3}$-replaced $Pb[(Zn_{1/3}Nb_{2/3}),Ti]O_3$ ceramics

Jee-Su Kim · Nam-Kyoung Kim

Received: 17 January 2006 / Accepted: 31 March 2006 / Published online: 28 December 2006

Abstract Octahedral lattice sites of $Pb[(Zn_{1/3}Nb_{2/3}),Ti]O_3$ were replaced by 20 at.% $Mg_{1/3}Ta_{2/3}$ complex to enhance perovskite development, especially at $Pb(Zn_{1/3}Nb_{2/3})O_3$-rich compositions. Resultant changes in the perovskite formation and associated dielectric responses were investigated. A perovskite structure was identified at $Pb(Zn_{1/3}Nb_{2/3})O_3$-rich compositions by X-ray diffraction, although the development was rather incomplete. Phase transition modes in the dielectric constant spectra changed from diffuse to sharp ones, regardless of the introduction of $Mg_{1/3}Ta_{2/3}$. Dielectric maximum temperatures of the ceramics shifted linearly with the compositional change.

Introduction

Lead zinc niobate $Pb(Zn_{1/3}Nb_{2/3})O_3$ (PZN) and lead magnesium tantalate $Pb(Mg_{1/3}Ta_{2/3})O_3$ (PMT) are complex-perovskite compounds, which exhibit frequency-dependent dielectric relaxation behavior along with diffuse modes in the phase transition [1–3]. In contrast, lead titanate $PbTiO_3$ (PT) is a simple perovskite with quite sharp phase transition in the dielectric constant spectra. Ceramic powders of perovskite PT and PMT can be prepared rather easily via direct or two-step calcination of constituent chemicals [4, 5]. Monophasic perovskite PZN, however, cannot be processed by any conventional solid-state reaction method under atmospheric pressure. Therefore, crystals and powders of perovskite PZN have been prepared with the aid of fluxes [6], under very high pressures [7], or via mechanochemical reaction routes [8].

Various physicochemical properties of $Pb(Zn_{1/3}Nb_{2/3})O_3$–$PbTiO_3$ (with/without additional components), especially near the morphotropic phase boundary, have been reported so far [9–13]. In the powder preparation, however, perovskite structure did not form at PZN-rich compositions, but only pyrochlores resulted instead [9] due to the rather strong covalency in PZN. Presence of unwanted pyrochlores in the perovskite matrix (even in small quantities) has been well reported to be quite detrimental to dielectric properties [14]. Therefore, it is essential to suppress/eliminate the pyrochlore formation in order to promote dielectric properties.

In the present study, therefore, 20 mol% PMT was introduced into the PZN-PT pseudobinary system in order to enhance perovskite development (especially at PZN-rich compositions) and to modify the associated dielectric responses at the same time. A two-step reaction route of the B-site precursor method [15, 16] (more comprehensive term for the so-called columbite process [17]) was employed in the present study. Instances of effective suppression of pyrochlore formation in lead-based complex-perovskite compositions can easily be found in the literature. Resultant perovskite developments and dielectric properties were investigated. Evolution of the internal microstructure was also examined.

J.-S. Kim · N.-K. Kim (✉)
Department of Inorganic Materials Engineering,
Kyungpook National University, 1370, Sankyuk-Dong,
Buk-Gu, Daegu 702-701, Korea
e-mail: nkkim@knu.ac.kr

Experimental

The 20 at.% $Mg_{1/3}Ta_{2/3}$-replaced Pb[$(Zn_{1/3}Nb_{2/3})$,Ti]O_3 compositions can be expressed as Pb[$(Mg_{1/3}Ta_{2/3})_{0.2}(Zn_{1/3}Nb_{2/3})_{0.8-x}Ti_x$]$O_3$, i.e., 0.2PMT–(0.8 – x)PZN–xPT. Starting materials were oxide chemicals of PbO (99.5%), MgO (99.9%), Ta_2O_5 (99.9%), ZnO (99.8%), Nb_2O_5 (99.9%), and TiO_2 (99.9%). Compositional stoichiometries were maintained as closely to the nominal values as possible by moisture compensation of the raw chemicals and of the separately synthesized precursor powders.

Powders of the B-site precursor system [$(Mg_{1/3}Ta_{2/3})_{0.2}(Zn_{1/3}Nb_{2/3})_{0.8-x}Ti_x$]$O_2$ were prepared by weighing, milling under ethyl alcohol (ZrO_2 media in a polyethylene container), drying, and calcination at 1050–1250°C for 2 h in air. The milling to calcination procedures were repeated once to promote phase development. PbO was then added to the synthesized precursor powders and the batches were milled, dried, and calcined 800–850 °C for 2 h. The calcined lumps were heat-treated again at 800–1050 °C for 2 h with intermediate milling and drying steps. Developed structures of the calcined powders were identified by X-ray diffraction (XRD, scanning speed = 4°2θ/min).

Prepared powders (with 2 wt% polyvinyl alcohol added as binder) were formed uniaxially into disk-type samples (10 mm diameter and ~3 mm thick), prior to further isostatic compaction at 100 MPa. The preforms were fired at 1050–1250 °C for 1 h in a multiple-enclosure crucible setup. Sintered pieces were ground and polished to attain parallel sides, onto which gold was sputtered for electrical contacts. Low-frequency (10^3–10^6 Hz) weak-field (~1 V_{rms}/mm) dielectric constant and loss values were measured on cooling (3–4 °C/min) using an impedance analyzer. The samples were then fractured and gold-coated, followed by further examination of internal microstructure using a scanning electron microscope (SEM).

Results and discussion

XRD results of the B-site precursor system [$(Mg_{1/3}Ta_{2/3})_{0.2}(Zn_{1/3}Nb_{2/3})_{0.8-x}Ti_x$]$O_2$ are displayed in Fig. 1. Only a columbite structure was identified at x = 0.0 and 0.2, whereas rutile was solely detected at the remaining composition range of x = 0.4–0.8. Since the two structures were not observed to coexist, it seems that any mutual dissolution between the columbite and rutile did not develop (at least over the composition interval of 0.2). Therefore, it can be speculated that a very narrow solubility range might exist at

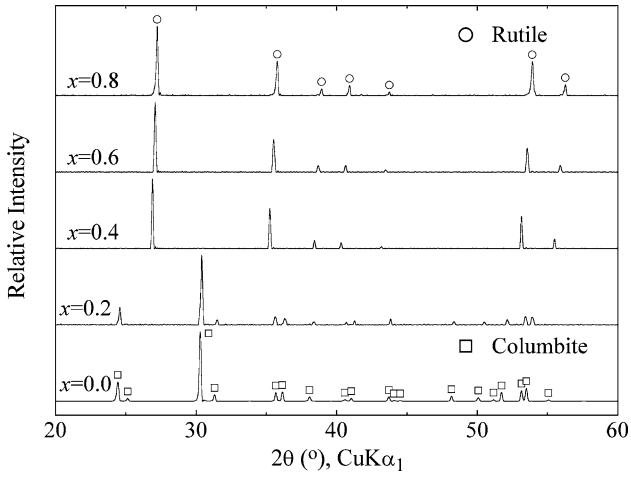

Fig. 1 Developed structures in the [$(Mg_{1/3}Ta_{2/3})_{0.2}(Zn_{1/3}Nb_{2/3})_{0.8-x}Ti_x$]$O_2$ B-site precursor system

$0.2 < x < 0.4$. Such rather insoluble nature between the two is believed to result from fundamentally dissimilar crystal structures, as reflected in the drastically different diffraction profiles.

The columbite structure ($x \le 0.2$) is not simply from $(Zn_{1/3}Nb_{2/3})O_2$ (i.e., $ZnNb_2O_6$, ICDD #37-1371), but rather incorporates 20 mol% $(Mg_{1/3}Ta_{2/3})O_2$ (trirutile, ICDD #32-631) and/or TiO_2 (rutile, ICDD #21-1276). Therefore, the two additional components must have been dissolved completely into the columbite structure. Likewise, the rutile is not from TiO_2 either, but theoretically of solid solutions formed from 0.4[$(Mg_{1/3}Ta_{2/3})_{1/2}Ti_{1/2}$]$O_2$ + 0.6TiO_2 and 0.4[$(Mg_{1/3}Ta_{2/3})_{1/2}Ti_{1/2}$]$O_2$ + 0.4[$(Zn_{1/3}Nb_{2/3})_{1/2}Ti_{1/2}$]$O_2$ + 0.2TiO_2 at x = 0.8 and 0.6, respectively. Powder diffraction files of the rutile-structured [$(Mg_{1/3}Ta_{2/3})_{1/2}Ti_{1/2}$]$O_2$ and [$(Zn_{1/3}Nb_{2/3})_{1/2}Ti_{1/2}$]$O_2$ are listed in ICDD #40-365 and #39-291. Similarly, the rutile of x = 0.4 could be either from 0.2$(Mg_{1/3}Ta_{2/3})O_2$ + 0.8[$(Zn_{1/3}Nb_{2/3})_{1/2}Ti_{1/2}$]$O_2$ or from 0.4[$(Mg_{1/3}Ta_{2/3})_{1/2}Ti_{1/2}$]$O_2$ + 0.4[$(Zn_{1/3}Nb_{2/3})_{1/2}Ti_{1/2}$]$O_2$ + 0.2$(Zn_{1/3}Nb_{2/3})O_2$. In either case, the 20 mol% components of $(Mg_{1/3}Ta_{2/3})O_2$ or $(Zn_{1/3}Nb_{2/3})O_2$ seemed to have been assimilated entirely to the host structure of rutile.

Developed structures in the 0.2PMT–(0.8 – x)PZN–xPT system are contrasted in Fig. 2. Pyrochlore and perovskite structures were observed to coexist at x = 0.0 (0.2PMT–0.8PZN). The development of perovskite (although incomplete) demonstrates the active role of PMT in the perovskite stabilization in PZN. Negligible fractions of PbO and ZnO were also identified at x = 0.0, which resulted seemingly from the formation of pyrochlore from powders of a perovskite stoichiometry. In contrast, only a perovskite structure was detected at $0.2 \le x$. Besides, a

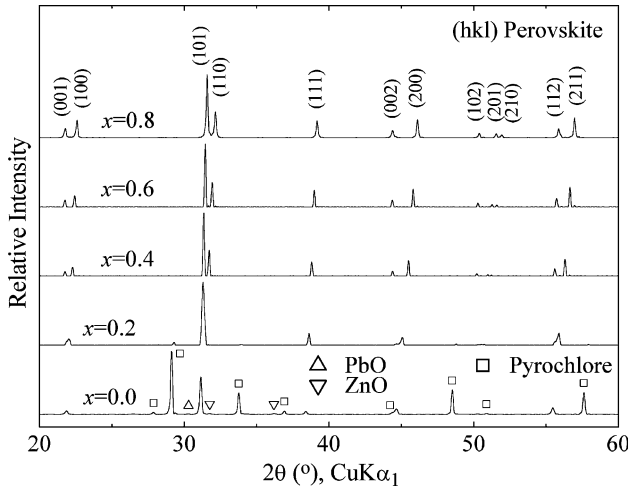

Fig. 2 X-ray diffraction results of the 0.2PMT–(0.8 – x)PZN–xPT system

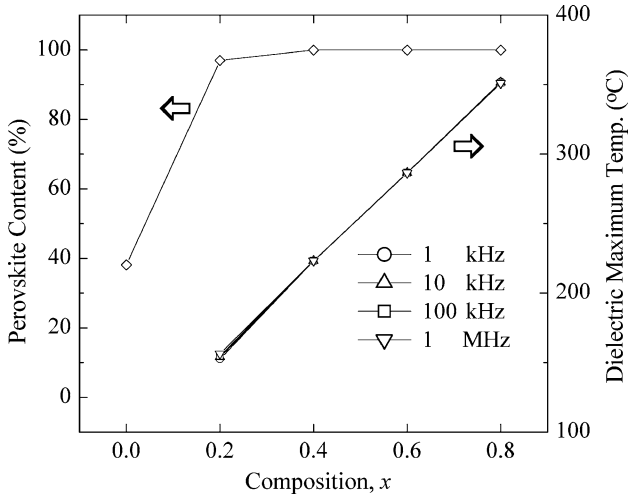

Fig. 3 Perovskite yields and dielectric maximum temperatures of the 0.2PMT–(0.8 – x)PZN–xPT system

(pseudo)cubic symmetry of the perovskite changed to tetragonal with further increase in PT fractions. Perovskite formation yields were determined from quantitative comparison between integrated intensities of the perovskite {110} and pyrochlore (222) reflections, $I_{\text{Perov.}}/(I_{\text{Perov.}} + I_{\text{Pyro.}})$, and the results are plotted in Fig. 3. As discussed previously, the values were only 38% at $x = 0.0$, but increased immediately to 98% ($x = 0.2$) and 100% ($0.4 \leq x$). Hence, pyrochlore formations were effectively suppressed by the introduction of $Mg_{1/3}Ta_{2/3}$ complex, except for $x = 0.0$. Relative densities of the ceramics were 94–96% of theoretical.

Temperature-dependent values of dielectric constant and loss of the 0.2PMT–(0.8 – x)PZN–xPT ceramics are shown in Fig. 4a. Dependencies upon measurement frequency are also shown in Fig. 4b, but only for two representative cases of $x = 0.2$ and 0.4 for simplicity. The dielectric constant values of $x = 0.0$ were quite low, 270–330 (at 1–1000 kHz) in the covered temperature range. Such low values can be directly attributed to the high fractions of pyrochlore (62%). Typical behavior of frequency-dependent relaxation in the dielectric constant and loss spectra (along with diffuse modes in the phase transition) is well demonstrated in $x = 0.2$, whereas such dispersion is hardly observable in $x = 0.4$ with very quite sharp phase transition modes. The spectra of $x = 0.6$ and 0.8 are basically similar to those of $x = 0.4$. Changes of the phase transition mode from diffuse to sharp ones with increasing PT fractions were also reported in PZN-PT [9]. Hence, the introduction of PMT in the present study did not appreciably influence the phase transition modes. The magnitude of the maximum dielectric constant of $x = 0.2$, $K_{\max} = 17{,}600$ (at 10 kHz), increased to 22,100 ($x = 0.4$) and 24,500 ($x = 0.6$), then decreased to 14,700 ($x = 0.8$). Variations of the

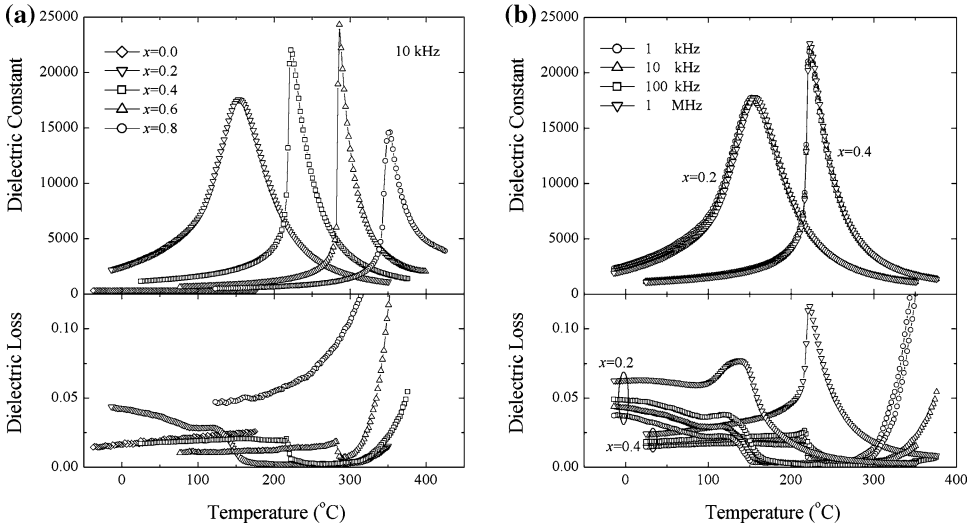

Fig. 4 Dielectric constant and loss values of the 0.2PMT–(0.8 – x)PZN–xPT ceramics (**a**) with frequency dependence (**b**)

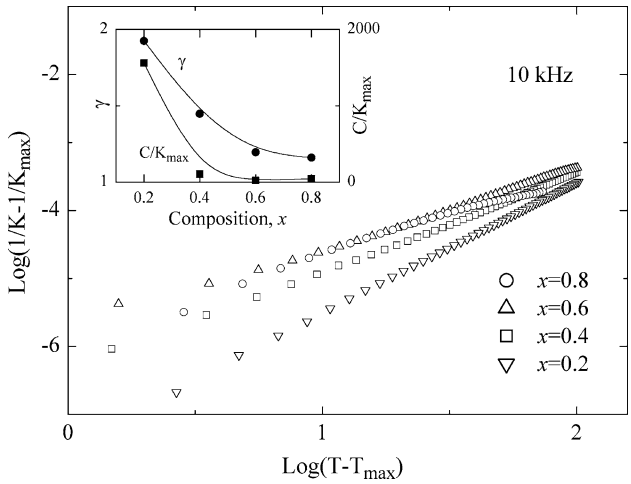

Fig. 5 Diffuseness parameters of γ and C/K_{max} (*inset*), determined from the plots of log $(1/K - 1/K_{max})$ versus log$(T - T_{max})$

dielectric maximum temperature (T_{max}) with compositional change are plotted in Fig. 3, where the values shifted fairly linearly. Meanwhile, the T_{max}-increase with increasing frequency ($T_{max,1\ MHz} - T_{max,1\ kHz}$) was 4 °C at $x = 0.2$, which decreased immediately to negligible values (<1 °C) at higher PT fractions.

Variations of the dielectric constant values (in the paraelectric temperature range) are often analyzed further to evaluate the diffuseness characteristics, details of which can be found elsewhere [5, 18–22]. The diffuseness exponent (γ) and degree of diffuseness (C/K_{max}) were evaluated from the slopes and intercepts of the log$(1/K - 1/K_{max})$ versus log$(T - T_{max})$ plots (Fig. 5) and the results are included in the inset. The comparatively high values of γ and C/K_{max} at $x = 0.2$ confirmed diffuse phase transition (as observed in the dielectric constant spectra). With increasing PT fractions, however, the two diffuseness parameters decreased to much smaller values (indicating sharp modes in the phase transition), consistent with the dielectric constant spectra (Fig. 4).

SEM images of the selected composition ceramics are shown in Fig. 6. The micrograph of $x = 0.0$ (not shown), where the perovskite yield was only 32%, consisted mostly of agglomerated pyrochlore grains with few scattered perovskite grains. At $x = 0.2$ (perovskite yield = 98%), however, occasional pyrochlore grains were dispersed preferentially along grain boundaries of the polyhedral perovskite. In contrast, only perovskite grains were observed at $x = 0.4$ and 0.6 (perovskite yield = 100%) with typical intergranular fracture modes. The micrograph of $x = 0.8$ (not shown) was similar to that of $x = 0.4$, except for somewhat undulated grain boundaries.

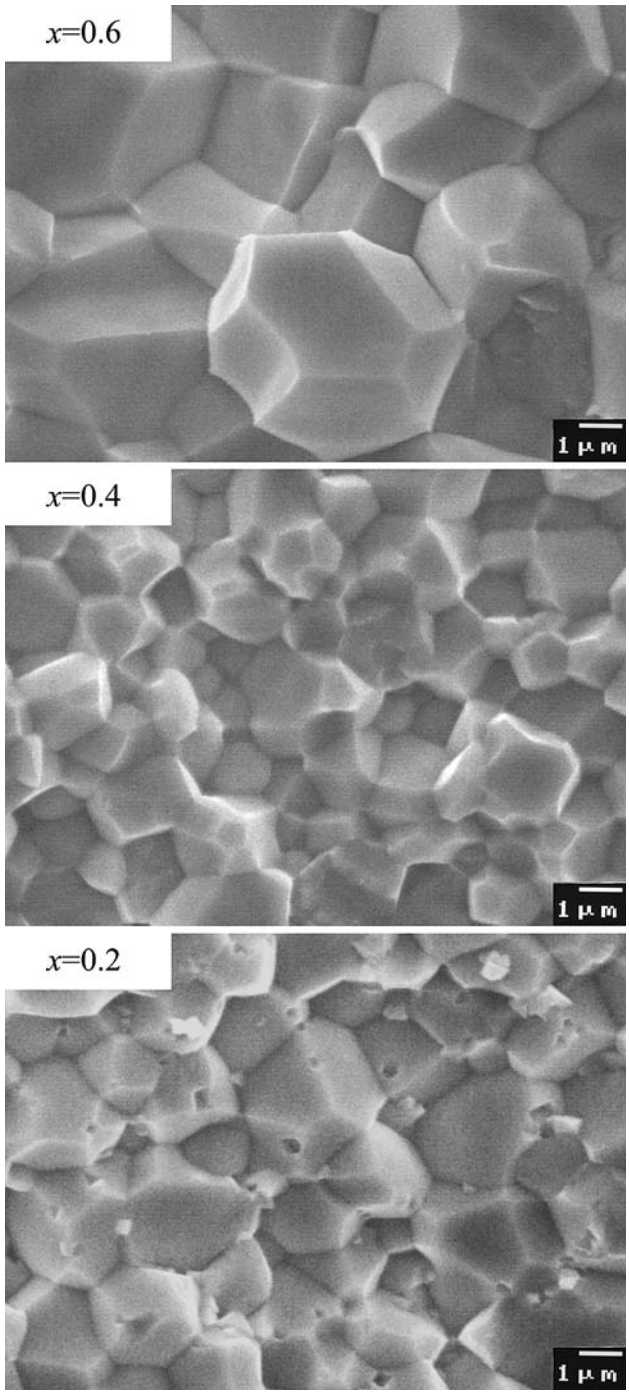

Fig. 6 Internal microstructure of fractured ceramics $x = 0.2$, 0.4, and 0.6

Summary

In the B-site precursor compositions of 0.2PMT–$(0.8 - x)$PZN–xPT, only columbite ($x = 0.0$ and 0.2) and rutile ($x = 0.4$–0.8) structures were identified without any apparent coexistence of the two. After the addition of PbO, by contrast, a perovskite structure

was solely detected in the entire composition range, except for the simultaneous presence of pyrochlore (along with negligible amounts of PbO and ZnO, too) at $x = 0.0$. Additionally, tetragonal symmetries of the perovskite developed gradually with increasing fractions of PT. The maximum dielectric constant values were highest (24,500 at 10 kHz) at $x = 0.6$, whereas corresponding temperatures increased virtually linearly with increasing PT fractions. Frequency-dependent dielectric relaxation (with diffuse phase transition) was observed at $x \leq 0.2$, whereas rather sharp modes were obtained at $0.4 \leq x$. Analysis results of the two diffuseness parameters (γ and C/K_{max}) confirmed the trends observed in the dielectric constant spectra, in terms of phase transition modes. Microstructure examination results of the sintered ceramics were generally consistent with the perovskite development yields.

Acknowledgement This study was supported by the Korea Research Foundation Grant (KRF-2001-041-E00456).

References

1. Bokov AA, Ye Z-G (2000) Solid State Commun 116:105
2. Chen IW (2000) J Phys Chem Solids 61:197
3. Zhu WZ, Mantas PQ, Baptista JL (2000) J Mater Sci Lett 19:491
4. Kim J-S, Kim N-K (2000) Mater Res Bull 35:2479
5. Lim S-M, Kim N-K (2000) J Mater Sci 35:4373
6. Bokov VA, Myl'nikova IE (1961) Sov Phys-Solid State 2:2428
7. Matsuo Y, Sasaki H, Hayakawa S, Kanamaru F, Koizumi M (1969) J Am Ceram Soc 52:516
8. Wang J, Wan D, Xue J, Ng WB (1999) J Am Ceram Soc 82:477
9. Lee D-H, Kim N-K (1998) Mater Lett 34:299
10. Jiang XP, Fang JW, Zeng HR, Chu BJ, Li GR, Chen DR, Yin QR (2000) Mater Lett 44:219
11. Kumar FJ, Lim LC, Chilong C, Tan MJ (2000) J Crystal Growth 216:311
12. Zhu WZ, Yan M, Kholkin AL, Mantas PQ, Baptista JL (2002) J Eur Ceram Soc 22:375
13. Bertram R, Reck G, Uecker R (2003) J Crystal Growth 253:212
14. Chen J, Gorton A, Chan HM, Harmer MP (1986) J Am Ceram Soc 69:C303
15. Shrout TR, Swartz SL, Haun MJ (1984) Am Ceram Soc Bull 63:808
16. Lee B-H, Kim N-K, Kim J-J, Cho S-H (1998) Ferroelectrics 211:233
17. Swartz SL, Shrout TR (1982) Mater Res Bull 17:1245
18. Uchino K, Nomura S (1982) Ferroelectrics Lett 44:55
19. Butcher SJ, Thomas NW (1991) J Phys Chem Solids 52:595
20. Kuwabara M, Takahashi S, Goda K, Oshima K, Watanabe K (1992) Jpn J Appl Phys 31:3241
21. Chae M-C, Lim S-M, Kim N-K (2000) Ferroelectrics 242:25
22. Ahn B-Y, Kim N-K (2000) J Am Ceram Soc 83:1720